ORIGINAL ARTICLE

High pressure equation of state for molten CaCO$_3$ from first principles simulations

Zhigang Zhang · Zairong Liu

Abstract Carbonate melts are important active metasomatic agents and efficient transport agents; their thermodynamic properties at high temperatures and pressures are therefore of considerable interest for various geochemical applications. However, due to the extreme challenges in relevant experiments, current knowledge of even the density of carbonate melts is limited. In this study, we provide high quality volumetric data of CaCO$_3$-melt from first principles at high temperatures and pressures (up to 3,500 K and 60 GPa). The accuracy of these data is demonstrated through comprehensive comparison with available experimental data and a thorough discussion of the predictability of the re-scaling method proposed in this study. Based on the simulations, an equation of state has been established that is critical to relevant highly disputed questions such as the decomposition and solidification boundaries of CaCO$_3$ melts, the latter of which is briefly discussed in this study with a newly derived ab initio melting curve to high pressures.

Keywords Carbonates · Melts · CaCO$_3$ · First principles · Equation of state

1 Introduction

Carbonate melts play important roles in various geochemical processes on the surface and in the interior of Earth (Jones et al. 2013). With remarkable features, such as

low density and high mobility, carbonate melts are well-known as active metasomatic agents in the mantle (Green and Wallace 1988). They are also recognized to be efficient transport agents of volatiles and rare earth elements due to the high solubility of these components in carbonate melts (Yang et al. 2003). In addition, carbonate melts are thought to be related to low seismic velocity and high electrical conductivity in the asthenosphere (Gaillard et al. 2008; Gudfinnsson and Presnall 2005) and to be responsible for the formation of "super-deep" diamonds (Litvin et al. 2014). Furthermore, shock-induced devolatilization of carbonate melts in Earth's early history dramatically alter the evolution of the atmosphere and may be the main cause for the Cretaceous–Tertiary extinction (O'Keefe and Ahrens 1989).

Despite the ubiquity and importance of carbonate melts, it is surprising to find that people actually know little about their properties at high temperatures and pressures, conditions under which carbonate melts often reside. Most experiments are concentrated around ambient pressure and mainly on alkali carbonate melts, owing to their role as electrolyte materials for fuel cells. Current measurements of carbonate melts are limited to 1,800 K and 5.5 GPa and significant discrepancies exist among different research groups, owing to the extreme challenges faced in these experiments (Dobson et al. 1996; Liu and Lange 2003).

Calcium-bearing carbonate melts are one of the main components of mantle-derived and highly evolved carbonatite melts (Church and Jones 1995). Nevertheless, as shown in Fig. 1, even the phase and stability boundaries of CaCO$_3$-melt remain poorly constrained. There is no consensus on exactly what temperature and pressure CaCO$_3$ liquid decomposes and what the products of its decomposition are in extreme conditions (Bobrovsky et al. 1976; Litvin et al. 2014; Martinez et al. 1995). Nor is there

Z. Zhang (✉) · Z. Liu
Key Laboratory of Earth and Planetary Physics, Institute
of Geology and Geophysics, Chinese Academy of Sciences,
Beijing 100029, China
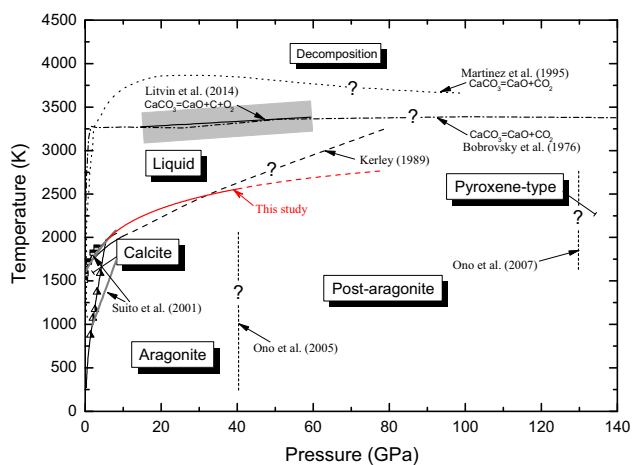e-mail: zgzhang@mail.iggcas.ac.cn

Fig. 1 Phase diagram of CaCO$_3$-system. *Points* at low temperatures and pressures are determined by Irving and Wyllie (1973) and Huang and Wyllie (1976), respectively, for calcite–aragonite transition and melting

consensus about the onset of melting of CaCO$_3$ solids and whether or not it is congruent (Kerley 1989; Spivak et al. 2011). Related with these, there is no consensus as to the precise boundary of crystalline phases and whether or not meta-stable polymorphs would be stabilized at high temperatures (Merlini et al. 2012; Oganov et al. 2006; Ono et al. 2005, 2007).

Uncertainty about CaCO$_3$ melts and their minerals, some of which are marked in Fig. 1, can be ascribed to the complexity of the structure and bonding of carbonates at high pressures (Oganov et al. 2013). Different from silicate melts, which are characterized by polymerization and network formation, carbonate melts consist of metal cations and carbonate CO$_3^{2-}$ anions with no definite association (Jones et al. 2013). The C–O bonds are more polarized and readily introduce more energetic local minimums by rotating the CO$_3^{2-}$ anions. This feature of carbonate melts calls for theoretical approaches from first principles; experimental measurements are extremely difficult and thermodynamic models with empirical parameters do not generate reliable predictions in regions far beyond the regression regime. For CaCO$_3$-melts, as shown in Fig. 1, the calculations by Bobrovsky et al. (1976), Kerley (1989), and Martinez et al. (1995) are thus prone to significant error at high pressures and temperatures.

Recently it has become our continuous endeavor to uncover the properties and roles of carbonatite melts in the mantle through first principles simulations based on predictive quantum mechanical theories. In this study, as an important step, we explore the pressure–volume–temperature (PVT) properties of CaCO$_3$-melts. Closely related to fundamental thermodynamic properties such as free energy and chemical potential, PVT properties are the key to solving the above-mentioned questions. In contrast to the

growing database of PVT data for fluids and silicate melts (Zhang and Duan 2005), high pressure PVT data of CaCO$_3$ melts are still extremely scarce. As a matter of fact, current knowledge of CaCO$_3$ melts is not remarkably better than that generated by studies carried out decades ago (Dobson et al. 1996; Genge et al. 1995; Liu and Lange 2003). With a generalized re-scaling method to correct the systematic errors in the simulation results (Zhang et al. 2013), we present an accurate equation of state (EOS) and, for the first time, extend the PVT data of CaCO$_3$-melts to at least 3,500 K and 60 GPa, rectifying the high pressure melting curve based on this EOS and that of the coexisting aragonite. Finally, we briefly discuss the implications of the results of this study.

2 Theory

2.1 Computational details

First principles simulations were carried out with Vienna ab initio simulation package (Kresse and Furthmuller 1996) using the projector-augmented-wave method (Kresse and Joubert 1999). We focused on the local density approximation (LDA) in most simulations and will show below that the results in this study will be essentially independent from the choices of exchange–correlation functional. Limited simulations with the PBE form of generalized gradient approximation (GGA; Perdew et al. 1996) have been performed for the purpose of comparison. The core radii are 2.3 atomic units (a.u.) for calcium (with a neon core), 1.5 a.u. for carbon (with a helium core), and 1.52 a.u. for oxygen (with a helium core).

We computed the thermodynamic and dynamical properties of molten CaCO$_3$ with extensive molecular dynamics (MD) simulations. At each time step (1 fs interval), the electronic structure was calculated at the Brillouin zone center with an energy cutoff of 500 eV and iteration convergence criterion of 10^{-6} eV. The thermal equilibrium between ions and electrons is assumed via the Mermin functional (1965). MD trajectories were propagated in the *NVT* ensemble with the Nosé thermostat (1984) for 7 ps, with the first 3 ps discarded as pre-equilibrium. Uncertainties in directly simulated quantities are determined using appropriate non-Gaussian statistics via the blocking method (Flyvbjerg and Petersen 1989). The primary cell is cubic with 160 atoms (32 formula units). The initial configurations were prepared through melting the 2 × 2 × 2 aragonite supercells by increasing the temperature and homogeneously straining the cell to a cubic shape. Simulation results for most properties were found to be unchanged within statistical uncertainties in larger systems (240 atoms) and durations twice as long.

Chin. J. Geochem. (2015) 34(1):13–20

15

We have not applied the quantum corrections for high temperature MD simulation results since the temperatures (>900 K) are much higher than the Debye temperature (<500 K for aragonite) and quantum effects should be negligibly small (Kerley 1989). On the other hand, in order to have accurate comparisons with experimental measurements at ambient conditions for crystals, as described in the next section, we counted the effects of zero-point vibrations by computing the phonon frequencies through the small displacement method with the aid of Phonopy (Togo et al. 2008). In these calculations, we relaxed the ionic structures with high precision (energy cutoff increased to 1,000 eV, iteration convergence criterion decreased to 10^{-8} eV) and dense k-point mesh ($5 \times 3 \times 4$ and $6 \times 5 \times 6$ for aragonite and post-aragonite, respectively). We used a $2 \times 2 \times 2$ supercell in calculating the force constant matrix by confirming its convergence for thermodynamic properties. Non-analytical-term corrections have been applied for longitudinal-transverse optical phonon frequency splitting in the limit of small wave-vector (Wang et al. 2010).

2.2 Systematic errors and corrections

Practical density functional theory (DFT) calculations rely on an approximation to the exchange–correlation functional. The two most widely used approximations: LDA and GGA, yield different predictions for quantities such as EOS. The main idea of a posteriori corrections to LDA and GGA is based on the observations that the correction to the energy should depend only on volume (van de Walle and Ceder 1999). A constant shift in pressure, named as the constant-shifting method hereafter, actually assumes the simplest possible volume-dependent form of correction to energy, i.e., linear with volume. Although popular for its simplicity, this method has been found to be insufficient to bring LDA and GGA predictions into agreement over a wide range of pressure. As discussed in Zhang et al. (2013), the alternative re-scaling method, achieved by counting the volumetric dependence of corrections in pressure, shows its superiority with high accuracy over the constant-shifting method.

A thermodynamic self-consistent derivation for the re-scaling method can be found in Zhang et al. (2013). We only briefly summarize here the formula involved in this study. In the mean time, by noticing that the corrections should be equivalent for the same stoichiometric system, as also argued by van de Walle and Ceder (1999), we further slightly generalize this method for situations beyond single phase.

The fundamental relation of the re-scaling method lies in the correction to the Helmholtz free energy:

$$
\begin{aligned}
F(V, T) &= F^{DFT}(V, T) + \Delta F_{ref}^{\exp - DFT}(V) \\
&= F^{DFT}(V, T) + \Delta F_{ref}^{\exp - DFT}(V_0) \\
&\quad + \left[\frac{V_0^{\exp} K_0^{\exp}}{V_0^{DFT} K_0^{DFT}} F_{ref}^{DFT}\left(V \frac{V_0^{DFT}}{V_0^{\exp}} \right) - F_{ref}^{DFT}(V) \right],
\end{aligned}
\tag{1}
$$

where subscript 0 refers to properties at zero pressure and an arbitrary reference temperature, K is the isothermal bulk modulus, and $\Delta F_{ref}^{\exp - DFT}(V_0) = F_{ref}^{\exp}(V_0^{\exp}) - \frac{V_0^{\exp} K_0^{\exp}}{V_0^{DFT} K_0^{DFT}} F_{ref}^{DFT}(V_0^{DFT})$ is the displacement of base free energy for the sake of re-scaling and can be neglected since relative (rather than absolute) free energy is concerned. Free energies with subscript ref represent those of a reference phase. When the reference temperature is selected as athermal (static) and focusing on a single phase, Eq. (1) is exactly that proposed in Zhang et al. (2013). The re-arrangement and slight generalization of Eq. (1) make it convenient to correct results for phases with few or even no experimental data since we can choose an alternative more familiar phase with the same stoichiometry as the reference phase. We will show in the next section that this generalization for $CaCO_3$-systems, though more or less empirical, is satisfactory for rendering DFT predictions independent of the form of the exchange–correlation functional and for agreeing with existing experimental measurements.

From the thermodynamic identity $P = -(dF/dV)_T$ we find from Eq. (1)

$$
\begin{aligned}
P(V, T) &= P^{DFT}(V, T) \\
&\quad + \left[\frac{K_0^{\exp}}{K_0^{DFT}} P_{ref}^{DFT}\left(V \frac{V_0^{DFT}}{V_0^{\exp}} \right) - P_{ref}^{DFT}(V) \right].
\end{aligned}
\tag{2}
$$

The constant-shifting method has also been applied to limited results to compare its performance with the above-mentioned re-scaling method. The correction to pressure reads

$$
\begin{aligned}
P(V, T) &= P^{DFT}(V, T) + P^{XC} \\
&= P^{DFT}(V, T) - P_{ref}^{DFT}(V_0^{\exp}).
\end{aligned}
\tag{3}
$$

The choices of parameters in these formulas are described in the caption of Fig. 4 in the next section.

3 Results and discussions

3.1 Structure

Finite sized MD simulations explore the phase space with constrained time and space scales. This somewhat hinders a quick downhill convergence to the global minimum, corresponding to the most stable phase, but on the other hand facilitates sampling meta-stable phase space and extends important information smoothly beyond the stable phases.

When the energy barriers between local minima are appropriate, phase transitions or chemical reactions can be observed in the MD trajectories. As for the simulation of $CaCO_3$-melts, we should ensure that in our sampling, (1) the melt has not crystallized at sufficiently low temperatures, and (2) the CO_3^{2-} has not completely decomposed into separate ions at sufficiently high temperatures. By inspecting the radial distribution function and the mean square displacement, we find the super-cooled $CaCO_3$-melt can be well sampled even deep within the solid phase regime (at least to 1,500 K and 50 GPa). The monitoring of decomposition is more ambiguous since the structure of $CaCO_3$-melt varies continuously over the temperatures and pressures. A first order inspection can be derived from the density of states, which is defined as the Fourier transformation of the velocity auto-correlation function (Allen and Tildesley 1987). As shown in Fig. 2, the crystalline phase of $CaCO_3$ (aragonite here) shows clear features in the high frequency region ($>500 \text{ cm}^{-1}$), which corresponds to that of normal modes of the carbonate group (Ni and Keppler 2013). The melting of the solid greatly destroys these features as revealed by the noticeable flattened spectra of super-cooled melt at the same temperature and volume. Increasing the temperature further blurs the characteristic peaks of frequency and at the temperature of 4,000–5,000 K it becomes essentially featureless. Therefore in the following discussions, we have not included the results at 4,000–5,000 K in order to eliminate any possible negative influence on the accuracy of EOS proposed in this study. We noticed that this approximate choice of temperature upper limit is consistent with a recent experiment, which demonstrates congruent melting of $CaCO_3$ at 3,500 K and 10–22 GPa (Spivak et al. 2011).

It is interesting to inspect more closely the equilibrated melt structure over varying temperatures and pressures. As shown in Fig. 3, we find significant effects on the local coordination environment from compressions, especially for Ca–O coordination. Over the pressures involved in this study, the structure varies continuously from calcite-like to post-aragonite-like, with Ca–O coordination increased from ~ 6.7 to ~ 10.3. This is inconsistent with that of the early classical simulations with force field by Genge et al. (1995), which finds a consistent similarity to calcite and may imply inaccuracy of their force field at high pressures. Variations of C–O coordination over pressure reveal subtle effects of compression on the carbonate groups. In Fig. 3a, we find the averaged C–O coordination number is generally equal to or slightly smaller than 3 except at extreme
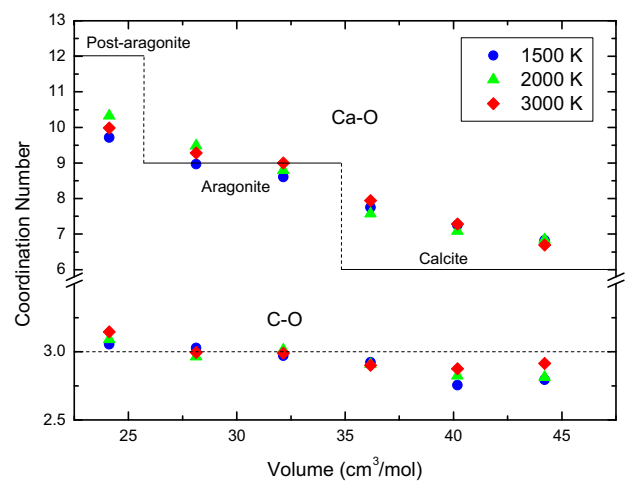
(a)
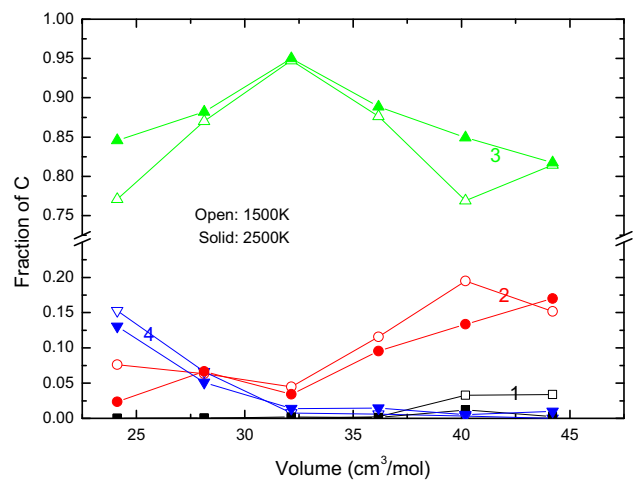
(b)

Fig. 3 **a** Ca–O and C–O coordination number at 1500, 2000, and 3000 K. The Ca–O coordination number of the crystalline phases with their approximate range of stability is shown for comparison. **b** Distribution of C–O coordination environments in $CaCO_3$ melts at 1,500 K (*open symbols*) and 2,500 K (*solid symbols*). *Numbers* denote the coordinated number of oxygen atoms around carbon
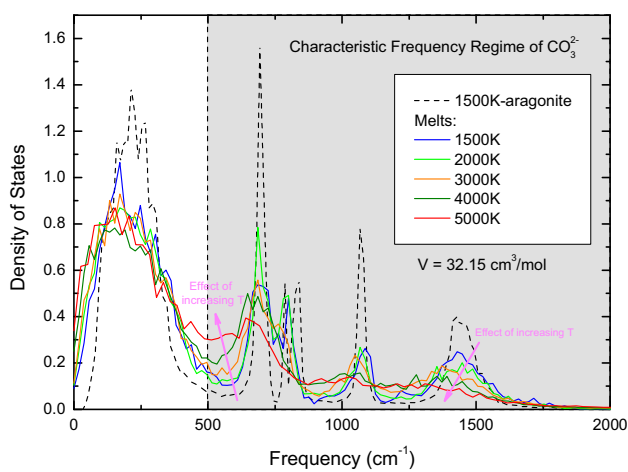

Fig. 2 Density of states (through Fourier transformation of velocity auto-correlation functions) of $CaCO_3$-melts at various temperatures with a volume of 32.15 cm³/mol. *Shaded area* represents the characteristic high frequency regime of carbonate anion. Aragonite at 1,500 K is included for comparison

high pressures. As shown in Fig. 3b, although the threefold C–O coordination dominates throughout the compression, the lower-than-threefold coordination (twofold or even onefold coordination at the lowest pressures inspected) always appears with 5–20 %. This feature is consistent with that proposed by Williams and Knittle (2003), who argued from their Raman spectroscopy that at least two anionic bonding environments exist in carbonate liquids with one carbonate-like bonding and the other single-bonded C–O units. At high pressures, the fourfold coordination gradually increases and the liquid structure is much more densely packed than solid phases, which only demonstrate CO_4^{4-} tetrahedral structures in the pyroxene-type phase with a pressure over 130 GPa (Oganov et al. 2006).

## 3.2 Corrections to the systematic DFT errors

We choose aragonite at 300 K as the reference phase and temperature for our re-scaling and also constant-shifting corrections, since we can find much more experimental data to show the accuracy of our corrections. Results for post-aragonite are included for comparison and to confirm our generalization of the re-scaling method proposed in this study for situations beyond the reference phase.

As shown in Fig. 4a, the predictions of LDA and GGA deviate from the experimental pressure by 3–7 GPa. LDA underestimates while GGA overestimates the pressures by similar amounts, which is in contrast to the comparisons for silicates, for which experimental pressures are much closer to LDA predictions (Zhang et al. 2013). The constant-shifting method is obviously inadequate to correct the deviations: even at modest pressure, the shifted GGA is larger than that of LDA by over 5 GPa.

In the inset plot of Fig. 4a and in Fig. 4b, we show the accuracies of the re-scaling method generalized in this study to a high temperature and a different phase, respectively. The corrections are unexpectedly extremely successful, with an almost exact match between re-scaled LDA and GGA predictions and perfect agreement with the available experimental data. The re-scaling method is demonstrated to be superior to the constant-shifting method with its high accuracy and independence of exchange–correlation functional, which is the major uncertainty in DFT simulations. All these comparisons convince us that we can also accurately predict PVT properties of $CaCO_3$-melt with a similar approach, as discussed in the following section.

3.3 EOS for $CaCO_3$-melt

After the re-scaling correction to the simulated results of melts, we established the EOS for $CaCO_3$-melt with the Mie–Gruneisen equation:
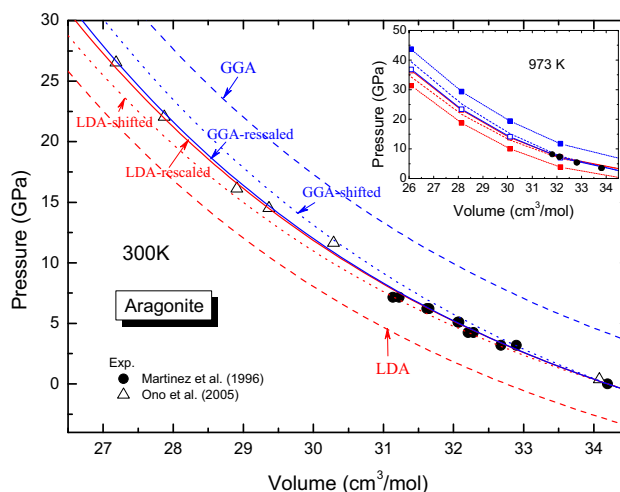
(a)
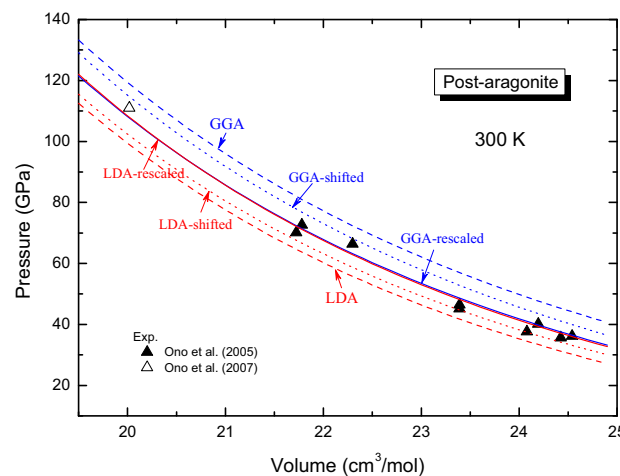
(b)

Fig. 4 High accuracy of the re-scaling method proposed in this study as revealed by comparison with experiments, and the predictions with the constant-shifting method for aragonite and post-aragonite. The parameters for the re-scaling are: $V_0^{exp} = 34.20$ cm³/mol and $K_0^{exp} = 67.1$ GPa (from those reported by Ono et al. 2005 for aragonite); $V_0^{LDA} = 32.75$ cm³/mol and $K_0^{LDA} = 75.0$ GPa; $V_0^{GGA} = 36.48$ cm³/mol and $K_0^{GGA} = 55.4$ GPa. For constant-pressure shifting, $P^{LDA} = 3.1$ GPa, $P^{GGA} = -4.4$ GPa
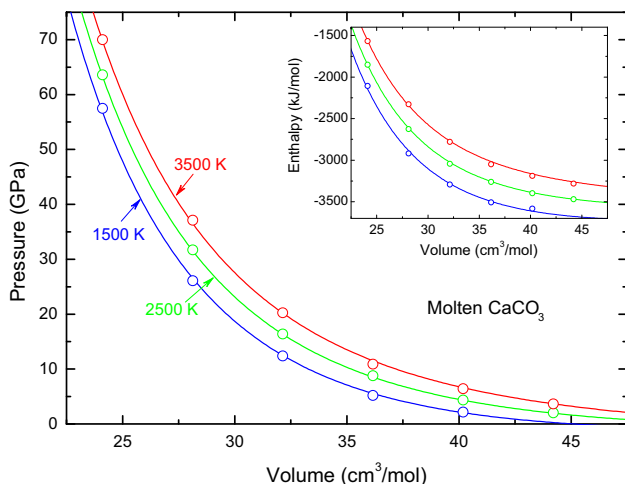
$$P(V,\ T) = P_C(V,\ T_0) + \frac{\gamma}{V} C_V (T - T_0),\qquad (4)$$

where P_C is the reference isotherm at $T_0 = 1{,}500$ K that can be accurately reproduced with a third-order Eulerian finite strain equation (known as Birch–Murnaghan equation), γ is the Gruneisen parameter which we simplify to be linear with V by $\gamma = \gamma_a + \gamma_b * (V - V_0)/40.1873$, and C_V is the isochoric heat capacity.

The parameters for this EOS are determined from linear least-square fitting and listed in Table 1. As shown in Fig. 5, the equation reproduces all the simulation results
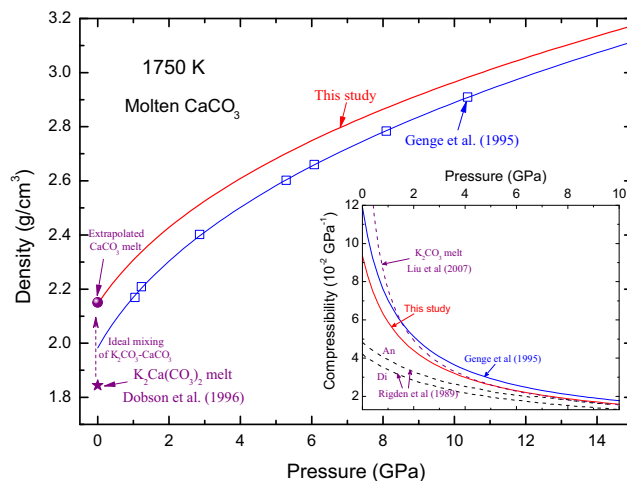
Table 1 Parameters for the equation of state (Eq. (4)) for molten CaCO₃ and aragonite at high temperatures and pressures

Parameters	Liquid	Aragonite
T_0 (K)	1,500	1,500
V_0 (cm³/mol)	45.14 ± 0.02	39.38 ± 0.02
K_0 (GPa)	11.87 ± 0.28	27.14 ± 0.33
K_0'	6.982 ± 0.202	6.014 ± 0.089
C_V/NR	3.180 ± 0.121	3.116 ± 0.169
γ_a	0.541 ± 0.051	1.077 ± 0.107
γ_b	−1.227 ± 0.024	0.359 ± 0.193
H_0 (kJ/mol)	−3,686.41 ± 8.90	−3,753.89 ± 4.37

Fig. 6 Density and isothermal compressibility of CaCO₃-melts at 1,750 K from different studies. *Blue lines* and *open squares* are those simulated by Genge et al. (1995) with empirical force field. Experimental measurement of K₂Ca(CO₃)₂ melt by Dobson et al. (1996) is shown a with *purple star* at the *bottom-left corner* of the plot. Assuming ideal mixing and utilizing density of K₂CO₃ determined by Liu and Lange (2003) at the same temperature and pressure, we get the density of CaCO₃ melt indicated by the *filled purple circle*. In the *inset* plot, we include the compressibility of K₂CO₃-melt determined by Liu et al. (2007), and those of anorthite (CaAl₂Si₂O₈) and diopside (CaMgSi₂O₆) melts measured by Rigden et al. (1989) for comparisons

Fig. 5 Equation of state for CaCO₃ melts. The simulated and corrected pressures and enthalpies (*inset*) at 1,500, 2,500, and 3,500 K are shown as *circles* with uncertainties smaller than the size of the *symbols*. The *lines* are Mie–Gruneisen equation of state (Eq. (4)) fitted to the simulation results with parameters listed in Table 1

quite well, including PVT properties (errors within 1 GPa) and energetic properties (errors within 1 %).

In Fig. 6, we show the predictability of this EOS by comparing it with experimental measurements. Although we can only find very limited experimental data about calcium-bearing carbonate melts relevant to this study (>1,500 K), some in-depth analyses may provide important information to assess the accuracy of this study. First, as argued by Liu and Lange (2003), carbonate components mix ideally, i.e., the volumes of carbonate liquids vary linearly with respect to the end-members. Secondly, although some systematic deviations exist between the measured densities of K₂Ca(CO₃)₂ melt by Liu and Lange (2003) and those by Dobson et al. (1996) at lower temperatures, we find they reach agreement at 1,750 K with a density of ∼1.82 g/cm³. Then with the well-determined density of K₂CO₃ melt at 1,750 K (1.67 g/cm³), we get the

extrapolated density of CaCO₃ melt to be 2.15 g/cm³ at ambient pressure and 1,750 K, which agrees with the prediction of our EOS in this study. In contrast, the predictions by classical MD simulations of Genge et al. (1995) systematically underestimate the densities over the pressures.

In the inset plot of Fig. 6, we computed the isothermal compressibility [defined as $\beta = 1/K_T = -(dV/dP)_T/V$] of CaCO₃ melt at 1,750 K. The results from this study are slightly smaller than those calculated by Genge et al. (1995). At low pressures, similar to K₂CO₃ (Liu et al. 2007), CaCO₃ melt can be more significantly compressed as compared with typical silicate melts such as anorthite (CaAl₂Si₂O₈) and diopside (CaMgSi₂O₆) melts (Rigden et al. 1989). With the increase of pressure to 10 GPa, the compressibility of carbonate melts rapidly decreases and all these melts interestingly show a similar magnitude of compressibility around 0.015 GPa⁻¹.

3.4 Applications and implications

The accurate EOS determined in this study has important applications related to calcium-bearing carbonatite melts. We only briefly introduce one as follows for the onset of melting CaCO₃ solids. For this purpose, we also calculated the EOS of CaCO₃–aragonite with the same approach mentioned above. The parameters of the aragonite are

listed in Table 1. We can predict the melting curve of CaCO$_3$ by integrating the Clausius–Clapeyron equation:

$$\frac{\partial T_m}{\partial P} = \frac{T \Delta V}{\Delta H}. \qquad (5)$$

Before the integration, we selected a converged experimental melting point at about 1,968 K and 5.5 GPa (Huang and Wyllie 1976; Suito et al. 2001). It should be noted that this point lies beyond calcite phase as revealed in Fig. 1 and mentioned by Irving and Wyllie (1973) and Ivanov and Deutsch (2002). From this fixed point and Eq. (4), we produced the melting curve of CaCO$_3$ over wide pressures in Fig. 7, which is the first curve from first principles, as far as we know. Compared with the early prediction by Kerley (1989), which has often been cited as the only melting curve before this study, we believe our results should be much more accurate for the reasons discussed above.

Based on the new derived melting curve, almost the whole bulk mantle falls into the solid regime of the CaCO$_3$ phase diagram, which implies that the calcium-dominant carbonate systems would not be melted over the entire mantle. To fuel the CaCO$_3$ minerals, extremely high heat flow is needed, which is often unlikely according to analysis of the global records (Pollack et al. 1993). The other possibility, which is more reasonable, would be eutectic melting through mixing with other components that have much lower melting temperatures. K$_2$CO$_3$, as an example, would be a good candidate to achieve the melting of CaCO$_3$. Again, assuming ideal mixing of the two

components, since the fusion curve of K$_2$CO$_3$ approaches the geotherm (Liu et al. 2007), we expect the carbonatite melts in the mantle should contain more alkali-bearing components than CaCO$_3$.

On the other hand, as shown in Fig. 7, it is possible that the melting curve of CaCO$_3$ meets with the geotherm at two points. In addition, as revealed in the inset plot of Fig. 7, we find the densities of CaCO$_3$ phases (liquid or solid) become even larger than that of diamond and the density contrast between the coexisting solid and liquid reduces significantly with increasing pressure. Oganov et al. (2008), by comparing the enthalpy change of relevant reactions, proposed that CaCO$_3$ becomes more prevalent in the lowermost part of the mantle. Combining all these factors, the most interesting speculation here is that we may find almost pure CaCO$_3$-melt at the base of the mantle. Of course, we should be aware that the unexplored phases (e.g., post-aragonite and pyroxene-type phase, as shown in Fig. 1) may (or may not) remarkably change the plausible extrapolation of the melting curve at high pressures (>40 GPa).

4 Conclusions

In this study, we present PVT properties of CaCO$_3$-melt at high temperatures and pressures (up to 3,500 K and 60 GPa) through extensive first principles simulations. To improve the accuracy and reliability of our predictions as much as possible, we carefully inspect the structures of melts to ensure proper sampling of the MD trajectories and comprehensively correct the systematic errors in the simulation results. Based on these efforts, we propose a high quality EOS for CaCO$_3$-melt at high pressures. From this equation, along with that of CaCO$_3$–aragonite, a melting curve has been obtained by integrating the Clausius–Clapeyron equation from first principles for the first time and plausibly implies the existence of CaCO$_3$-melt at the base of the mantle.

Fig. 7 Melting curve predicted in this study and those by experimental measurements (Huang and Wyllie 1976; Suito et al. 2001) and by thermodynamic model of Kerley (1989). Melting data of K$_2$CO$_3$ by Liu et al. (2007) and Klement and Cohen (1975) are shown on the *left-bottom* of the diagram. Temperature profile over the mantle is picked from Ono (2008). In the *inset* plot, we compare the density of the coexisting solid and liquid densities and the density of diamond at 2,603 K (Suzuki et al. 1998) is included for comparison

References

Allen MP, Tildesley DJ (1987) Computer simulation of liquids. Clarendon Press, Oxford

Bobrovsky SV, Gogolev VM, Zamyshlyaev BV, Lozhkina VP, Rasskazov VV (1976) The study of thermal decomposition influence on the spallation velocity for strong shock waves in solids. Fiz Tech Probl Razrab Polezn Iskop 3:49–57
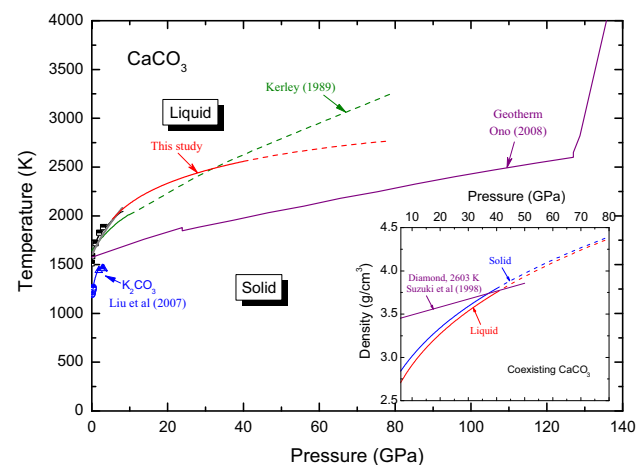
20

Chin. J. Geochem. (2015) 34(1):13–20

Church AA, Jones AP (1995) Silicate–carbonate immiscibility at Oldoinyo-Lengai. J Petrol 36:869–889

Dobson DP, Jones AP, Rabe R, Sekine T, Kurita K, Taniguchi T, Kondo T, Kato T, Shimomura O, Urakawa S (1996) In-situ measurement of viscosity and density of carbonate melts at high pressure. Earth Planet Sci Lett 143:207–215

Flyvbjerg H, Petersen HG (1989) Error-estimates on averages of correlated data. J Chem Phys 91:461–466

Gaillard F, Malki M, Iacono-Marziano G, Pichavant M, Scaillet B (2008) Carbonatite melts and electrical conductivity in the asthenosphere. Science 322:1363–1365

Genge MJ, Price GD, Jones AP (1995) Molecular-dynamics simulations of $CaCO_3$ melts to mantle pressures and temperatures—implications for carbonatite magmas. Earth Planet Sci Lett 131:225–238

Green DH, Wallace ME (1988) Mantle metasomatism by ephemeral carbonatite melts. Nature 336:459–462

Gudfinnsson GH, Presnall DC (2005) Continuous gradations among primary carbonatitic, kimberlitic, melilititic, basaltic, picritic, and komatiitic melts in equilibrium with garnet lherzolite at 3–8 GPa. J Petrol 46:1645–1659

Huang W-L, Wyllie PJ (1976) Melting relationships in the systems $CaO–CO_2$ and $MgO–CO_2$ to 33 kilobars. Geochim Cosmochim Acta 40:129–132

Irving AJ, Wyllie PJ (1973) Melting relationships in $CaO–CO_2$ and $MgO–CO_2$ to 36 kilobars with comments on CO_2 in the mantle. Earth Planet Sci Lett 20:220–225

Ivanov BA, Deutsch A (2002) The phase diagram of $CaCO_{(3)}$ in relation to shock compression and decomposition. Phys Earth Planet Inter 129:131–143

Jones AP, Genge M, Carmody L (2013) Carbonate melts and carbonatites. Carbon Earth 75:289–322

Kerley GI (1989) Equations of state for calcite minerals. I. Theoretical model for dry calcium carbonate. High Press Res 2:29–47

Klement W, Cohen LH (1975) Solid–solid and solid–liquid transitions in K_2CO_3, Na_2CO_3 and Li_2CO_3—investigations to greater than −5 kbar by differential thermal-analysis—thermodynamics and structural correlations. Ber Bunsenges Phys Chem 79:327–334

Kresse G, Furthmuller J (1996) Efficient iterative schemes for ab initio total-energy calculations using a plane-wave basis set. Phys Rev B 54:11169–11186

Kresse G, Joubert D (1999) From ultrasoft pseudopotentials to the projector augmented-wave method. Phys Rev B 59:1758–1775

Litvin Y, Spivak A, Solopova N, Dubrovinsky L (2014) On origin of lower-mantle diamonds and their primary inclusions. Phys Earth Planet Inter 228:176–185

Liu Q, Lange RA (2003) New density measurements on carbonate liquids and the partial molar volume of the $CaCO_3$ component. Contrib Mineral Petrol 146:370–381

Liu Q, Tenner TJ, Lange RA (2007) Do carbonate liquids become denser than silicate liquids at pressure? Constraints from the fusion curve of K_2CO_3 to 3.2 GPa. Contrib Mineral Petrol 153:55–66

Martinez I, Deutsch A, Scharer U, Ildefonse P, Guyot F, Agrinier P (1995) Shock recovery experiments on dolomite and thermodynamical calculations of impact-induced decarbonation. J Geophys Res Solid Earth 100:15465–15476

Merlini M, Hanfland M, Crichton WA (2012) $CaCO_3$-III and $CaCO_3$-VI, high-pressure polymorphs of calcite: possible host structures for carbon in the Earth's mantle. Earth Planet Sci Lett 333:265–271

Mermin ND (1965) Thermal properties of inhomogeneous electron gas. Phys Rev 137:1441

Ni HW, Keppler H (2013) Carbon in silicate melts. Rev Mineral Geochem 75:251–287

Nosé S (1984) A molecular-dynamics method for simulations in the canonical ensemble. Mol Phys 52:255–268

O'Keefe JD, Ahrens TJ (1989) Impact production of CO_2 by the Cretaceous/Tertiary extinction bolide and the resultant heating of the Earth. Nature 338:247–249

Oganov AR, Glass CW, Ono S (2006) High-pressure phases of $CaCO_3$: crystal structure prediction and experiment. Earth Planet Sci Lett 241:95–103

Oganov AR, Ono S, Ma YM, Glass CW, Garcia A (2008) Novel high-pressure structures of $MgCO_3$, $CaCO_3$ and CO_2 and their role in Earth's lower mantle. Earth Planet Sci Lett 273:38–47

Oganov AR, Hemley RJ, Hazen RM, Jones AP (2013) Structure, bonding, and mineralogy of carbon at extreme conditions. Carbon Earth 75:47–77

Ono S (2008) Experimental constraints on the temperature profile in the lower mantle. Phys Earth Planet Inter 170:267–273

Ono S, Kikegawa T, Ohishi Y, Tsuchiya J (2005) Post-aragonite phase transformation in $CaCO_3$ at 40 GPa. Am Mineral 90:667–671

Ono S, Kikegawa T, Ohishi Y (2007) High-pressure transition of $CaCO_3$. Am Mineral 92:1246–1249

Perdew JP, Burke K, Ernzerhof M (1996) Generalized gradient approximation made simple. Phys Rev Lett 77:3865–3868

Pollack HN, Hurter SJ, Johnson JR (1993) Heat flow from the Earth's interior: analysis of the global data set. Rev Geophys 31:267–280

Rigden SM, Ahrens TJ, Stolper EM (1989) High-pressure equation of state of molten anorthite and diopside. J Geophys Res Solid Earth 94:9508–9522

Spivak AV, Dubrovinskii LS, Litvin YA (2011) Congruent melting of calcium carbonate in a static experiment at 3500 K and 10–22 GPa: its role in the genesis of ultradeep diamonds. Dokl Earth Sci 439:1171–1174

Suito K, Namba J, Horikawa T, Taniguchi Y, Sakurai N, Kobayashi M, Onodera A, Shimomura O, Kikegawa T (2001) Phase relations of $CaCO_3$ at high pressure and high temperature. Am Mineral 86:997–1002

Suzuki A, Ohtani E, Kato T (1998) Density and thermal expansion of a peridotite melt at high pressure. Phys Earth Planet Inter 107:53–61

Togo A, Oba F, Tanaka I (2008) First-principles calculations of the ferroelastic transition between rutile-type and $CaCl_{(2)}$-type $SiO_{(2)}$ at high pressures. Phys Rev B 78:134106

van de Walle A, Ceder G (1999) Correcting overbinding in local-density-approximation calculations. Phys Rev B 59:14992–15001

Wang Y, Wang JJ, Wang WY, Mei ZG, Shang SL, Chen LQ, Liu ZK (2010) A mixed-space approach to first-principles calculations of phonon frequencies for polar materials. J Phys Condens Matter 22:202201

Williams Q, Knittle E (2003) Structural complexity in carbonatite liquid at high pressures. Geophys Res Lett 30:1022. doi:10.1029/2001GL013876

Yang XM, Yang XY, Zheng YF, Le Bas M (2003) A rare earth element-rich carbonatite dyke at Bayan Obo, Inner Mongolia, North China. Mineral Petrol 78:93–110

Zhang ZG, Duan ZH (2005) Prediction of the PVT properties of water over wide range of temperatures and pressures from molecular dynamics simulation. Phys Earth Planet Inter 149:335–354

Zhang ZG, Stixrude L, Brodholt J (2013) Elastic properties of $MgSiO_3$-perovskite under lower mantle conditions and the composition of the deep Earth. Earth Planet Sci Lett 379:1–12